Molecular Immunology 47 (2010) 726–737

Contents lists available at ScienceDirect

Molecular Immunology

journal homepage: www.elsevier.com/locate/molimm

Structural and functional comparison of MIF ortholog from *Plasmodium yoelii* with MIF from its rodent host

Dingding Shao[a,1], Xiang Zhong[a,1], Yan-Feng Zhou[b,2], Zhifu Han[a,3], Yahui Lin[a], Zhensheng Wang[a], Lingyi Bu[a], Lianhui Zhang[a], Xiao-Dong Su[b,*], Heng Wang[a,**]

[a] *Department of Microbiology and Parasitology, Institute of Basic Medical Sciences, Chinese Academy of Medical Sciences and School of Basic Medicine, Peking Union Medical College, 5# Dong Dan 3 Tiao, Beijing, 100005, China*
[b] *National Laboratory of Protein Engineering and Plant Genetic Engineering, Peking University, Beijing, 100871, China*

ARTICLE INFO

Article history:
Received 25 June 2009
Received in revised form 22 October 2009
Accepted 22 October 2009
Available online 8 December 2009

Keywords:
Macrophage migration inhibitory factor
Malaria
Tautomerase activity
Crystal structure
ERK1/2

ABSTRACT

Host-derived macrophage migration inhibitory factor (MIF) has been implicated in the pathogenesis of malaria infection, especially in malarial anemia. Although two *Plasmodium* parasite-derived MIF orthologs, *Plasmodium falciparum* MIF and *P. berghei* MIF were identified recently, the crystal structure and the precise roles of *Plasmodium*-derived MIFs, particularly in combination with the host MIF, remain unknown. In this study, we identified another MIF ortholog from a rodent-specific *P. yoelii* (PyMIF). This molecule shares a conserved three-dimensional structure with murine MIF (MmMIF), but with a different substrate binding pattern and much lower tautomerase activity. It could activate host cells via several signaling pathways *in vitro*, and inhibiting macrophage apoptosis, also similarly to MmMIF. However, we found that PyMIF and MmMIF acted synergistically to activate the MAPK-ERK1/2 signaling pathway at very low concentration but acted antagonistically at higher concentration. Furthermore, we detected PyMIF in the sera of infected mice and found that injection of recombinant PyMIF (rPyMIF) during infection could up-regulate several pro-inflammatory cytokines *in vivo* and slightly delay the death of infected mice. These data suggest that PyMIF modulates host immune responses together with host MIF and has potential to prolong parasitemia or the chronicity of malaria infection.

1. Introduction

Malaria is one of the most deadly human infectious diseases in the world, affecting more than 200 million people and causing nearly one million deaths each year. Malaria control is hampered by the occurrence of drug-resistant parasites, the absence of an effective vaccine, and limited knowledge of parasite biology, malaria pathology, and the host immune response to parasite infection. Malaria parasites can complete their life cycle despite inducing a host immune attack. It has been hypothesized that these parasites can modulate the host immune response to the benefit of their own life cycle. In recent years, sequencing of the genomes of humans and *Plasmodium* parasites has improved our understanding of parasite biology and host immunity, and some *Plasmodium* parasite-derived molecules, such as macrophage migration inhibitory factor (MIF), have been identified as potential modulators of host immune cell activity.

Host-derived MIF has been considered a crucial cytokine in innate and acquired immunity against infectious diseases. During malarial parasite infection, the level of circulating host MIF is altered relative to the level in non-infected individuals (Awandare et al., 2007; Fernandes et al., 2008; McDevitt et al., 2006). In a mouse model of malaria, the circulating level of host MIF during *Plasmodium chabaudi* infection correlates with disease severity (Martiney et al., 2000). Further, host MIF is found to play a critical role in the pathogenesis of malarial anemia (Martiney et al., 2000; McDevitt et al., 2006). All of the above indicate that host MIF is a critical inflammatory response-associated molecule during malaria infection that also participates in immunopathology. In addition, host MIF plays either a protective or a deleterious role in the immune response to many different pathogens. For instance, host MIF plays a detrimental role during lethal *L. monocytogenes* infection (Sashinami et al., 2006), whereas it seems to promote development of a protective immune response against infections by *Salmonella typhimurium* (Koebernick et al., 2002), *Leishmania major* (Juttner et al., 1998;

* Corresponding author. Tel.: +86 10 62759743.
** Corresponding author. Tel.: +86 10 65296440; fax: +86 10 65237921.
E-mail addresses: yanfengzhou.pku@gmail.com (Y.-F. Zhou), hanzhifu0807@163.com (Z. Han), xdsu@pku.edu.cn (X.-D. Su), wanghpumc@gmail.com (H. Wang).
[1] These authors contributed equally to this work.
[2] Present address: Immune Disease Institute, Harvard Medical School, Boston, MA 02215, USA.
[3] Present address: National Institute of Biological Sciences, Beijing, 102206, China.

0161-5890/$ – see front matter © 2010 Elsevier Ltd. All rights reserved.
doi:10.1016/j.molimm.2009.10.037

Satoskar et al., 2001), *Taenia crassiceps* (Rodriguez-Sosa et al., 2003), and *Toxoplasma gondii* (Flores et al., 2008).

In recent years, a number of parasite-derived MIF orthologs (identified from nematode, hookworm, *Leishmania,* and *Plasmodium*) have been identified and found to have almost identical structure and similar biological activity as mammalian MIFs (Augustijn et al., 2007; Cho et al., 2007; Cordery et al., 2007; Kamir et al., 2008; Pastrana et al., 1998; Shao et al., 2008; Tan et al., 2001; Zang et al., 2002). In serum specimens of infected humans, people have found not only antibodies against *Brugia malayi* MIF (BmMIF) (Zang et al., 2002) and *P. falciparum* MIF (PfMIF) (Cordery et al., 2007), but also PfMIF molecule itself (Shao et al., 2008). The existence of the molecule and its antibody in host circulation indicate that the parasite MIF must be an important modulator of the host immune response.

Here, we report the identification of a new malaria parasite-derived MIF, *P. yoelii* MIF (PyMIF). Following sequence and crystal structure analysis, we investigated the role of PyMIF in activating host immune cells in combination with MmMIF and its *in vivo* functions in modulating the host cytokine network during malaria infection. Our results help to improve understanding of the biological activity of malaria parasite-derived MIFs, the parasite–host interaction, and may help to elucidate the mechanisms of host protection and parasite evasion.

2. Materials and methods

2.1. Mice and experimental infection

Female Balb/c mice 6–8 weeks of age were used for all experiments. Mice were housed in the experimental animal center of the Institute of Basic Medical Sciences, Peking Union Medical College, under specific-pathogen-free conditions. Lethal *P. yoelii 17XL* malaria parasites were maintained in Balb/c mice. Infections were initiated by intraperitoneal injection of 2×10^5 *P. yoelii*-infected erythrocytes. The parasitemia of individual mice was monitored via blood smears stained with Giemsa. The PyMIF levels in the sera were determined by PyMIF-specific sandwich ELISA (described below).

2.2. Cloning of PyMIF cDNA

P. yoelii-infected Balb/c mice with 30% parasitemia were sacrificed, and arterial blood was collected for RNA extraction. RNA was isolated using TRIzol Reagent (Invitrogen) and cDNA was synthesized using the M-MLV kit (Promega). The sequence coding for PyMIF was amplified by polymerase chain reaction (PCR) using PyMIF-specific primers: PyE111new (5′-GGAATTCCATATGCCTTGCTGCGAATTAAT-3′) and PyE302 (5′-CCCTCGAGGCCAAATAGTGAACCACTAAAAGC-3′). The PCR product was cloned in-frame into pET30b (Invitrogen) using the NdeI and XhoI restriction sites. To generate polyclonal antibodies, the PyMIF open reading frame was PCR-amplified with primers PyG1new (5′-CGGGATCCATGCCTTGCTGCGAATTAAT-3′ with a 5′-BamHI restriction site) and PyG2 (5′-CCGCTCGAGTTAGCCAAATAGTGAACCACT-3′ with a 5′-XhoI restriction site); then the PCR product was cloned in-frame into pGEX-4T-1 (GE Healthcare) using the BamHI and XhoI restriction sites

2.3. Preparation of recombinant MIF proteins

Recombinant plasmids were transformed into *Escherichia coli* BL21 (DE3), and expression of the recombinant histidine-tagged PyMIF (PyMIF-His) and the recombinant GST-tagged PyMIF (PyMIF-GST) were induced by addition of 0.625 mM isopropyl-β-D-thiogalactopyranoside to the bacterial culture for 3.5 h at 37 °C. PyMIF-His was purified using a nickel-agarose column (Ni-NTA Agarose, Invitrogen). For biological assays, the recombinant MIF was eluted with elution buffer (250 mM imidazole in 25 mM Tris–HCl [pH 7.8] and 50 mM NaCl). The eluted proteins were dialyzed against NaH_2PO_4–Na_2HPO_4 phosphate buffer [pH 7.8]. The protein concentrations were determined using the BCA™ Protein Assay Kit (Pierce), and the purity exceeded 95%. Endotoxin was removed from the recombinant protein solutions as described previously (Bernhagen et al., 1994). Briefly, the MIF-containing fractions were applied to a C8-SepPak reverse-phase (RP) column (Waters) and MIF was eluted with 60% acetonitrile/water, frozen at −80 °C, lyophilized. For renaturation, MIF was dissolved at a concentration of 200–400 μg/ml in 20 mM sodium phosphate buffer (pH 7.8) containing 8 M urea and 5 mM DTT and dialyzed against 20 mM sodium phosphate buffer (pH 7.8) containing 5 mM DTT followed by 20 mM sodium phosphate buffer (pH 7.8) alone. Renatured MIF was sterile-filtered and kept at 4 °C until use. The lipopolysaccharide content in the MIF preparations was determined by chromogenic *Limulus* amoebocyte assay. Lipopolysaccharide contamination in the recombinant MIF proteins was 0.025 EU/μg of protein. For crystallization assays, the recombinant protein was eluted via nickel-agarose chromatography using elution buffer (250 mM imidazole in 25 mM Tris–HCl [pH 8.5] and 50 mM NaCl) and then applied to Source Q (GE Healthcare) anion-exchange columns, followed by Superdex 200 gel filtration chromatography (GE Healthcare). The PyMIF-GST was purified using Glutathione Sepherose™ 4B (GE Healthcare). The protein concentrations were determined using the BCA™ Protein Assay Kit (Pierce), and the purity exceeded 95%.

For the native PAGE, 4 μg recombinant MmMIF-His and 4 μg recombinant PyMIF-His were separated on an 8% polyacrylamide gel [pH 8.8] under native condition and visualized with Coommassie blue staining. Protein molecular weight standards for native PAGE were myoglobin equine (17.8 kDa), albumin egg (45.0 kDa), albumin bovine (BSA) (67.0 kDa), catalase bovine (240.0 kDa) and Ferritin horse (450.0 kDa) (Serva). The proteins from an identical gel were transferred to a PVDF membrane and immunostained with anti-PyMIF monoclonal antibody 3E2 (described below).

2.4. Tautomerase assays

The protocol for the *p*-hydroxyphenylpyruvate (HPP) tautomerase assay has been described previously (Swope et al., 1998). Briefly, the substrate HPP was dissolved in 50 mM ammonium acetate (pH 6.0) and the recombinant MIF protein was dissolved in boric acid (pH 6.2). The enzymatic activity was determined at 25 °C by adding 50 μl of 0.2 mM HPP solution to a quartz vessel containing 50 μl MIF solution; absorbance was measured at 330 nm.

2.5. Generation of anti-PyMIF polyclonal and monoclonal antibodies

Anti-PyMIF-GST polyclonal antibodies (pAbs) were generated in rabbits and anti-PyMIF-His monoclonal antibody (mAb) 3E2 (IgG2a isotype) was produced in mice according to standard protocols. All antibodies were purified using recombinant Protein A Sepharose Fast Flow (GE Healthcare) and dialyzed against PBS.

2.6. PyMIF-specific sandwich ELISA

The level of PyMIF in the sera of malaria-infected mice was measured by PyMIF-specific sandwich ELISA, similar to the host MIF ELISA method described previously (Martiney et al., 2000). Briefly, 96-well ELISA plates were coated with 1.5 μg of the anti-PyMIF mAb (clone 3E2, IgG2a isotype) in PBS overnight at room temperature. The plates were washed with Tris-buffered saline

(TBS)–0.05% Tween 20, and blocked with TBS containing 2% goat serum for 1 h at 37 °C. Then, 100 μl of the samples were plated and incubated for 1 h at 37 °C. The plates were then washed and the anti-PyMIF pAb (diluted 1:250) was added and incubated for 1 h at 37 °C. After washing, alkaline phosphatase-conjugated goat anti-rabbit IgG (1:1000 dilution; Beijing Zhongshan Goldenbridge Biotechnology Co., Ltd.) was added for 1 h at 37 °C. Finally, the substrate, *p*-nitrophenyl phosphate in ethanolamine solution was added and positive signals were read at 405 nm. PyMIF concentrations were determined using a standard curve obtained from known concentrations of recombinant PyMIF (14.8–60,800 pg/ml) included in each assay plate. The lower limit of detection was 238 pg/ml.

2.7. Crystallization and data collection

Superdex 200 gel filtration-purified recombinant PyMIF-His protein was in buffer containing 100 mM NaCl and 10 mM Tris–HCl [pH 8.5]. Crystallization was carried out using the hanging drop vapor diffusion method. Crystals of PyMIF were prepared by mixing equal volumes of protein solution with well buffer containing 2.5 M ammonium sulfate and 0.1 M sodium acetate (pH 4.6). For production of the PyMIF and HPP complex, one day prior to data collection, powdered HPP was dusted into the mother liquid with crystals of PyMIF. X-ray diffraction data sets for both the apoPyMIF and PyMIF in complex with HPP were collected at beamline 3W1A in the Beijing Synchrotron Radiation Facility. Crystals were cryoprotected using well buffer containing 15% DMSO and then flash-frozen in liquid nitrogen before mounting into the 100 K nitrogen stream. For both sets of data, 140° oscillation ranges were collected with 1° per frame width. Data sets were integrated and scaled using XDS and XSCALE (Kabsch, 1993). The collected data are presented in supporting Table S1.

2.8. Structure determination and refinement

The structure of apoPyMIF was determined by molecular replacement using MOLREP (Vagin and Teplyakov, 1997) with the Protein Data Bank code entry ID (1MFI) as the search model. Six monomers in one asymmetric unit were arranged as two trimers. Structure refinement was performed using Refmac5 (Winn et al., 2001), and manual adjustment of the model was done in Coot (Emsley and Cowtan, 2004). Non-crystallographic symmetry restraints were used in the early stage of refinement and the restraints were loosened in later refinement cycles; no non-crystallographic symmetry restraint was applied in the final model. When R_{free} decreased to 0.28, TLS refinement was performed and TLS groups were selected according to TLSMD (Painter and Merritt, 2006). The final *R* factor and R_{free} were 0.177 and 0.208, with no outliers in the Ramanchandran plot.

The structure of the PyMIF/HPP complex was phased by MOLREP using one of the trimers in the final apo structure. Refinements were carried out similarly to the process for apo structure determination, and HPP molecules were located according to the Fo-Fc difference map in the last step of refinement. In the final model, the *R* factor and R_{free} were 0.154 and 0.190, with no outliers in the Ramanchandran plot. Refinement statistics are shown in Table S1.

2.9. Cell culture

RAW264.7 cells and NIH/3T3 cells were obtained from the Cell Culture Center of the Institute of Basic Medical Sciences/Chinese Academy of Medical Sciences. Cells were cultured in high-glucose Dulbecco's modified Eagle's medium (DMEM) supplemented with 10% fetal calf serum (FCS; Hyclone), 100 units/ml penicillin-streptomycin, and 4 mM L-glutamine at 37 °C and 5% CO_2

2.10. Western analysis of MAPK/ERK, PI3K/AKT, and JAK/STAT activation and apoptosis-related assays

MAPK/ERK, PI3K/AKT, and JAK/STAT activation assays were performed as described previously (Lue et al., 2007). Two hundred thousand NIH/3T3 fibroblasts were plated in 12-well cell culture plates in DMEM/10% FCS for 24 h. Medium was exchanged for DMEM/0.5% FCS and then cells were starved for 24 h before treatment with PyMIF or MmMIF alone or PyMIF plus MmMIF at various concentrations for 20 min. Cells were harvested and lysed in ice-cold NP-40 lysis buffer containing 1% Nonidet P-40, 10 mM Tris–HCl (pH 8.0), 150 mM sodium chloride, 2 mM ethylenediaminetetraacetic acid, 100 μg/ml dithiothreitol, and 1 mM phenylmethylsulfonyl fluoride. Protein extracts were separated via 12% SDS-PAGE and transferred to nitrocellulose membranes or polyvinylidene difluoride membranes (Millipore). The membrane was probed with anti-p-Akt (Ser473)/Akt, anti-p-Jak2 (Tyr1007/1008)/Jak2, and anti-p-Tyk2 (Tyr1054/1055)/Tyk2, antibodies from the phosphoPlus P44/P42 MAP Kinase (Thr202/Tyr204) Antibody Kit and p-Stat/Stat Antibody Sampler Kit (Cell Signaling Technology), followed by peroxidase-conjugated anti-rabbit IgG (Zhongshan Goldenbridge Biotechnology Co., Ltd.). Densitometric analysis was performed using AlphaEaseFC. One million RAW 264.7 cells were cultured in 12-well plates in DMEM supplemented with 0.5% FCS in the presence or absence of PyMIF or MmMIF at 100 ng/ml, with or without ISO-1 (MIF inhibitor, Merck) for 20 h; western analysis was performed as described above using anti-cleaved caspase 9, anti-cleaved caspase 3, and anti-cleaved PARP antibodies (Apoptosis Antibody Sampler Kit, Cell Signaling Technology).

2.11. Luciferase assay for monitoring AP-1 and NF-κB activation

AP-1 reporter gene activity was measured in NIH/3T3 cells as described previously (Kleemann et al., 2000). Two hundred nanograms of pAP-1 luciferase reporter plasmid and 4 ng pRenilla control plasmid (Clontech) were transfected into NIH/3T3 cells using lipofectamine 2000 (Invitrogen). After transfection, incubations with recombinant PyMIF or control buffer were carried out for 18 h, followed by an 8-h co-incubation with 3 nM phorbol myristate 13-acetate (PMA; Merck). Cells were harvested and luciferase and Renilla activities were measured according to the manufacturer's protocol (dual-luciferase reporter assay system, Promega). Measurements of NF-κB reporter gene activity were carried out as described above, except that recombinant PyMIF was added for 40 h.

2.12. Annexin V and propidium iodide staining

RAW264.7 cells were cultured in 12-well plates at 1×10^6 cells/well in DMEM supplemented with 0.5% FCS with or without MIFs or 2 μM ISO-1 for 18 h. Cells were collected by centrifugation, washed, and stained using the Annexin V-FITC Apoptosis Detection Kit (Beyotime) and analyzed by flow cytometry.

2.13. RNA isolation and reverse transcription

Total RNA was isolated from cultured RAW264.7 macrophage cells using TRIzol Reagent (Invitrogen). Reverse transcription was carried out using Superscript II RT (Invitrogen). Primers used were BCL-2: 5′- TGTGTGTGGAGAGCGTCAAC and 3′-GGCCATATAGTTCCACAAAG; BCL-xL: 5′-ACTGTGCGTGGAAAGCGTAG and 3′-ATCCACAAAAGTGTCCCAGC; BAX: 5′-GCTACAGGGTTTCATCCAGG and 3′-ATTGCTGTCCAGTTCATCTC;

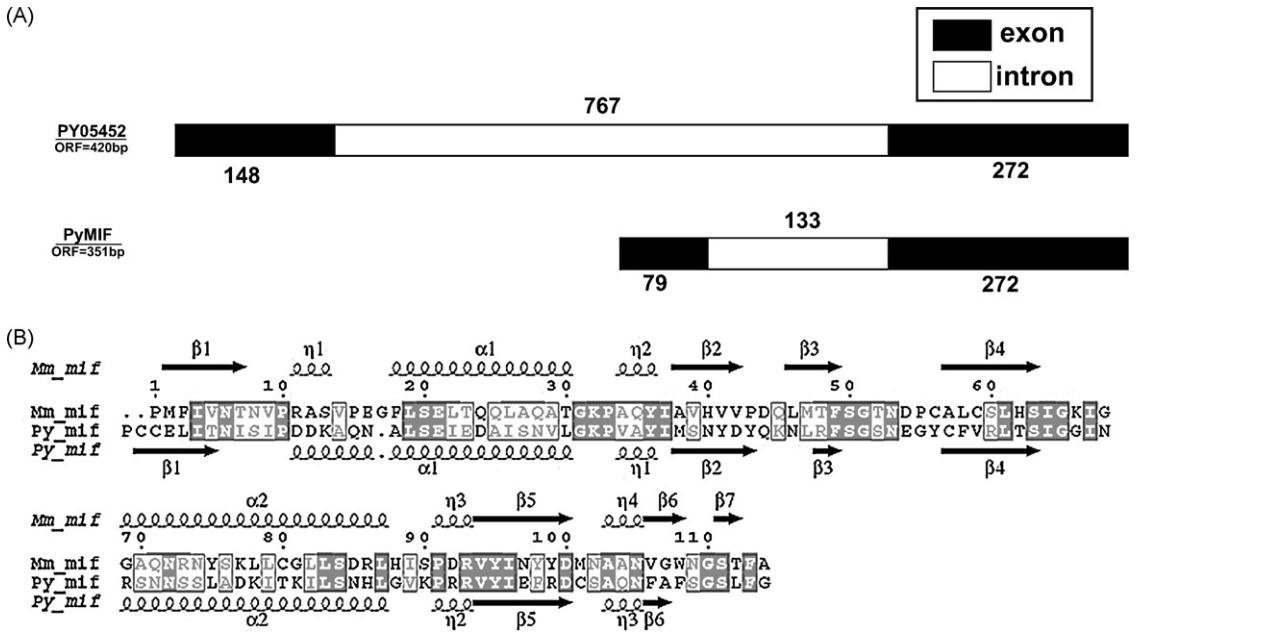

Fig. 1. (A) Genomic organization of the predicted and verified PyMIF gene. Introns are shown as open boxes and exons are filled boxes. The size of each region (in bases) is indicated above introns and beneath exons. (B) Alignment of the amino acid sequence and secondary structure assignments of crystalline PyMIF and MmMIF. Residues that are highlighted in white with gray background shown identity, conserved residues are highlighted gray with white backgruod. (α1–α2), (β1–β7), and (η1–η4) represent α helices, β strands, and η helices in the secondary structure, respectively.

HPRT: 5′-TCATTATGCCGAGGATTTGG and 3′-CCCCCCTTGAGCACACAGAG. Densitometric analysis was performed using AlphaEaseFC.

2.14. Animal experiments and cytokine detection

Balb/c mice were challenged with *P. yoelii* as described above, intravenously injected with 200 ng of recombinant PyMIF or ovalbumin (OVA) once on day 4 or 5, or once each on days 4 and 5. The parasitemia of individual mice was monitored on blood smears stained with Giemsa. In addition, cytokine levels were determined in the twice-injected mice at 36 h post-last injection. The cytokines IL-12p70, TNF-α, IFN-γ, MCP-1, IL-10, and IL-6 in the sera of mice were determined according to the manufacturer's protocol (Mouse Inflammation Kit, BD^{TM} Cytometric Bead Array).

2.15. Statistical analysis

Data are expressed as mean values ± standard deviation. The statistical significance of differences was evaluated by analysis of variance using SPSS 11.01. Tukey's test was used for post hoc comparisons of specific groups. Statistical significance was determined at $p < 0.05$.

3. Results

3.1. PyMIF in the circulation of P. yoelii-infected mice

The sequence of the MIF ortholog in the *P. yoelii* genome is the same as that of the gene initially described to encode a hypothetical protein (Gene Bank Number PY05452). The predicted protein sequence consists of 139 amino acids and differs significantly from the sequence of any other MIF molecules. We corrected the PyMIF open reading frame, which consists of two exons (79 and 272 bp) and encodes a 116-amino acid protein (Gene Bank Number DQ494171, Fig. 1A), by analyzing the gene sequence and blasting the *P. yoelii* genome against PfMIF and MIFs derived from several other organisms. The revised amino acid sequence of PyMIF shares 30% identity with (48% positive) murine MIF (MmMIF) and 76% identity with (91% positive) PfMIF (Fig. 1B).

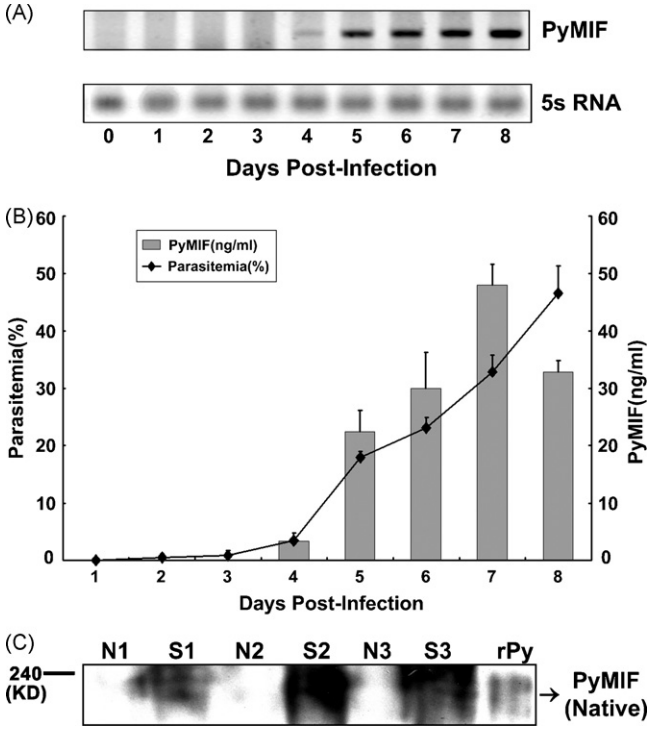

Fig. 2. Expression of PyMIF in infected mice. (A) The transcription level of the *PyMIF* gene detected in the spleen of infected mice during the process of infection; 5S RNA was used for standardization. (B) Expression level of PyMIF in the sera of infected mice during the process of infection as measured by sandwich ELISA. (C) PyMIF protein in the serum of infected mice (N represents control healthy mice; S represents infected mice; 1,2 and 3 represent different mice, and the sera from infected mice were collected on the 6th day post-infection) as determined by native PAGE western analysis. rPy represents recombinant PyMIF protein.

Table 1
Tautomerase activity of PyMIF and MmMIF.

Substrate	MIF	Specific activity (μmol/min/mg)[a]
p-Hydroxyphenylpyruvate	MmMIF	393.86 ± 41.10
	PyMIF	10.87 ± 1.18 (2.76%[b])

[a] The specific activities were determined five times per protein and the results are presented as the average and mean ± standard deviation of five determinations.
[b] The numerical value is the percentage of the specific activity of PyMIF relative to that of MmMIF.

The PyMIF transcript was detected in mouse peripheral blood from day 4 post-challenge with lethal *P. yoelii* strain 17XL (Fig. 2A). To determine whether PyMIF existed in the circulation system of infected mice, we developed mAb 3E2 that recognizes a specific conformational determinant of the PyMIF molecule and shows no cross-reactivity with MmMIF (Fig. S1). Using this mAb and a PyMIF-specific pAb in a specific sandwich ELISA, we detected PyMIF in the sera of each infected mouse, including two inbred strains (BALB/c and C57BL/6 mice) and one outbred strain (KM mice) (data not shown). Furthermore, we detected PyMIF protein in the serum of infected mice beginning at day 4 and increasing up to day 7, when parasitemia was about 30% (Fig. 2B). Meanwhile, using the PyMIF-specific pAb, bands specific for PyMIF in the serum of infected mice were detected by native PAGE western analysis (Fig. 2C).

3.2. Crystal structure of PyMIF

To understand the relationship between human and malaria parasite MIFs, we determined the crystal structures of apoPyMIF and PyMIF in complex with HPP at 1.8 and 2.1 Å, respectively. As defined by the crystallography data (Table S1), an asymmetric unit consisted of two trimers of PyMIF monomers. Despite only 30% amino acid identity, PyMIF was highly conserved in secondary and tertiary structure with MmMIF (Fig. 1B and Fig. 3A). Each monomer contained two α helices and a four-stranded β sheet. The trimer was stabilized by inter-subunit interactions between the carboxyl-terminus of one monomer and one helix of the other and between the β sheets from nearby subunits. The root mean square deviation for main chain atoms between PyMIF:HPP and MmMIF (1MFI) was 1.0 $Å^2$.

Interestingly, there was a significant difference in the substrate binding pattern between PyMIF and mammalian-derived MIFs. Comparing with the crystal structure of HuMIF in complex with HPP (PDB ID 1CA7), the orientation of HPP in the PyMIF active site was opposite (Fig. 3B and Fig. S2). By analyzing the amino acids in the active site, we found that four of five amino acids important for substrate binding or catalytic activity in the HuMIF active site (Pro 2, Lys 34, Ile 66, and Tyr 97′) (prime stands for residue from neighboring chain in the trimer) were conserved in PyMIF. However, Glu99′ in PyMIF was substituted for Asn97′ in HuMIF. Furthermore, Phe108 in Pymif, instead of a much shorter Val106 in

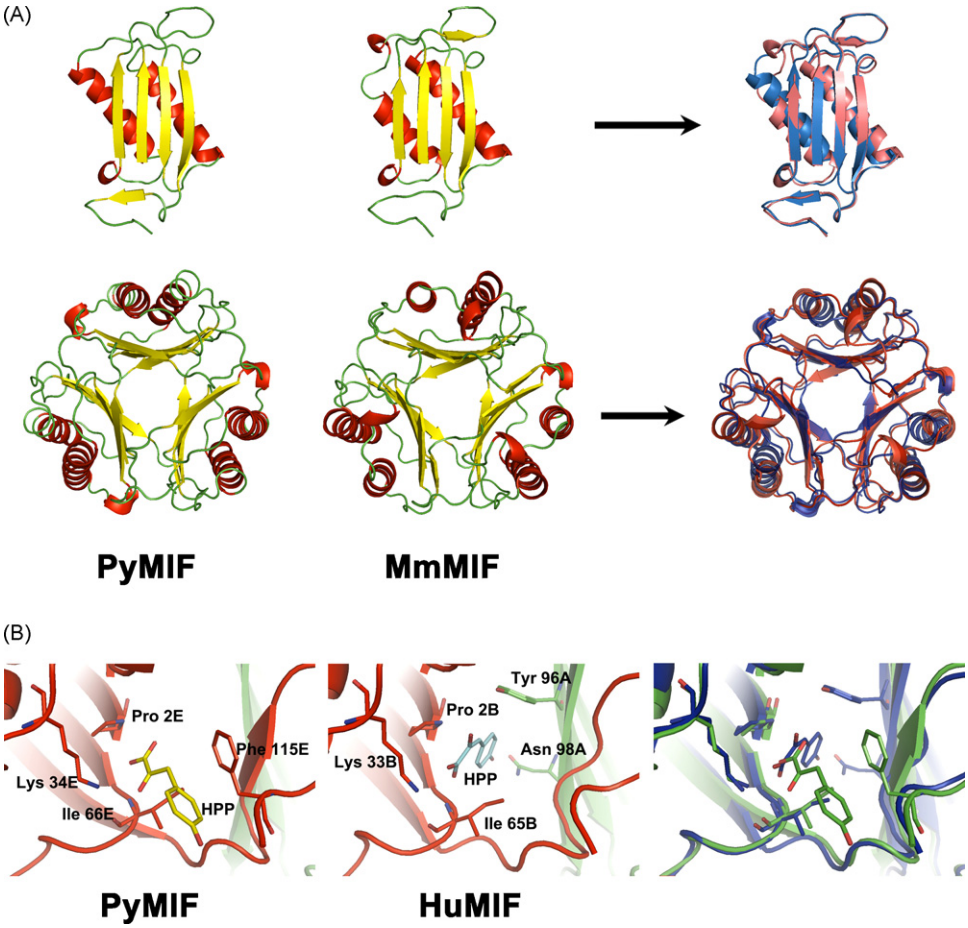

Fig. 3. Structural comparison of PyMIF and host MIF. (A) Schematic representation of the PyMIF and MmMIF monomers (top) and trimers (bottom) with secondary structure elements shown in yellow (β-sheet), red (α-helix), and green (random coil). The right side shows the superposition of the backbone of monomeric and trimeric PyMIF (blue) and MmMIF (red). (B) Comparing the active sites of PyMIF (left) and HuMIF (middle) and their superposition (right). The active site residues in the crystal structure of PyMIF:HPP and HuMIF:HPP (PDB ID: 1CA7) are shown in stick presentation. Two adjacent monomers are presented in red and green (left and middle). HPP is displayed in yellow in the crystal structure of PyMIF:HPP (left), and in blue in the crystal structure of HuMIF:HPP (middle). PyMIF with HPP and HuMIF with HPP were respectively colored in green and blue in superposition (right).

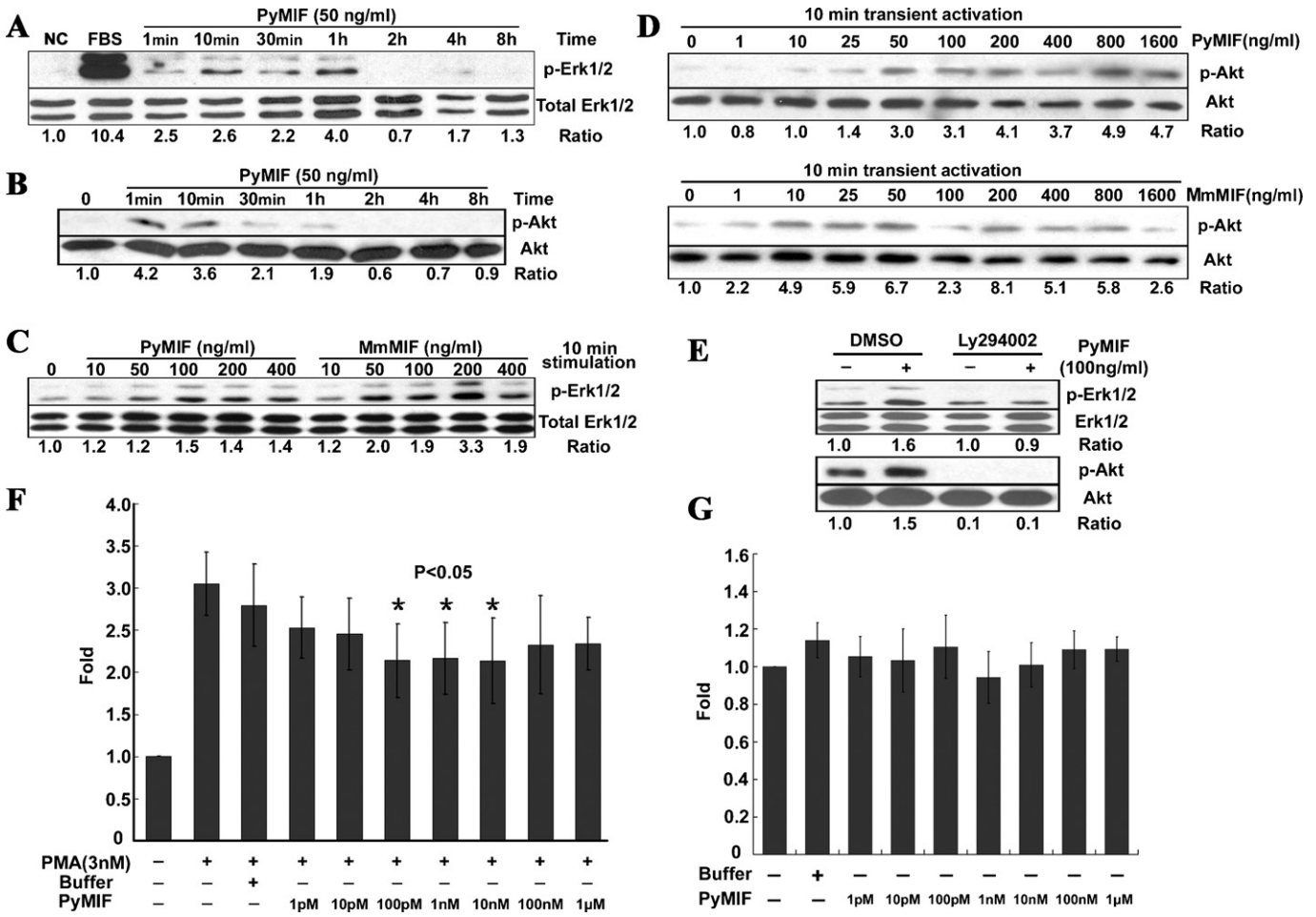

Fig. 4. PyMIF activates PI3K-AKT and MAPK pathways. (A andB) Time course of endogenous Erk1/2 and Akt phosphorylation induced by 50 ng/ml recombinant PyMIF. Total Erk1/2 or Akt protein was used for standardization, respectively. Numbers indicate relative phosphorylation ratios. (C and D) Dose–response of the phosphorylation of Erk1/2 and Akt induced by 10 min treatment with recombinant PyMIF and recombinant MmMIF. Total Erk1/2 or Akt protein was used for standardization, respectively. Numbers indicate relative phosphorylation ratios. (E) Dependence of recombinant PyMIF-stimulated Akt activation on PI3K and partial inhibition of recombinant PyMIF-stimulated ERK1/2 signaling by PI3K inhibitors. Results shown are representative blots of three independent experiments. (F) PyMIF showed statistically relevant repression of AP-1 transcription induced by PMA at the concentration extent between 100 pM and 10 nM compared to buffer controls. Asterisks indicate $p < 0.05$ ($n = 6$). (G) PyMIF showed a non-significant trend toward elevating NF-κB transcription in NIH/3T3 cells and mouse embryonic fibroblasts (MEFs) as compared to buffer controls ($n = 4$).

HuMIF, will clash with the head group of HPP (Fig. S3). In PyMIF, the reoriented head group of HPP led the main interacting amino acids locating on one chain, including Pro 2, Lys 34, Ile 66 and Phe 115 (Fig. 3B). To determine the effect of this change to the catalytic site on enzyme function, we compared the tautomerase activities of PyMIF and MmMIF on HPP and found that the specific activity of PyMIF was far lower than that of MmMIF (Table 1). The change in the binding site sequence could be related to the decreased HPP tautomerase activity.

3.3. PyMIF and host MIF have similar effects on signal transduction

To investigate the host regulatory pathways mediated by PyMIF, we first evaluated its activity in the MAPK/ERK and PI3K/AKT pathways in the well-characterized NIH/3T3 cell line. PyMIF induced a significantly rapid and transient phosphorylation of both Erk1/2 and Akt (Fig. 4A and B). Notably, maximum phosphorylation of Akt occurred at 1 min, demonstrating kinetics similar to those of MmMIF (Gore et al., 2008). PyMIF-induced phosphorylation of both Erk1/2 and Akt was lower than that of MmMIF (Fig. 4C and D). The chemical PI3K inhibitor Ly294002 completely suppressed PyMIF-induced phosphorylation of Akt (Fig. 4E), indicating that Akt activation by PyMIF was dependent on PI3K, again similar to host MIF. Moreover, Erk1/2 phosphorylation by PyMIF could be weakened by Ly294002 (Fig. 4E), also similar to host MIF (Lue et al., 2007).

Recently, Augustijn et al. reported that PfMIF and PbMIF could reduce AP-1 expression, partially dependent on the oxidoreductase activity of MIF (Augustijn et al., 2007). We also found that PyMIF could reduce PMA-induced expression of AP-1 at PyMIF concentrations of 100 pM–10 nM (Fig. 4F), which is within the concentration range detected in the sera of infected mice. This result indicated that physiologically relevant concentrations of PyMIF could modulate AP-1. Furthermore, using a gene reporter system, we found no significant effect of PyMIF on NFκB activity in fibroblast cells (Fig. 4G), although the role of host MIF on NF-κB signaling pathway remains controversial (Amin et al., 2006). In addition, we investigated the effect of PyMIF on the JAK-STAT pathway. Western analysis showed that neither PyMIF nor MmMIF could phosphorylate several signaling molecules in JAK-STAT pathway, such as Jak2, Tyr2, Stat3, or Stat5 (Fig. S4). In addition, no typical Jak- or Stat-dependent gene expression was found to be induced by PyMIF or MmMIF in microarray analysis (data not shown).

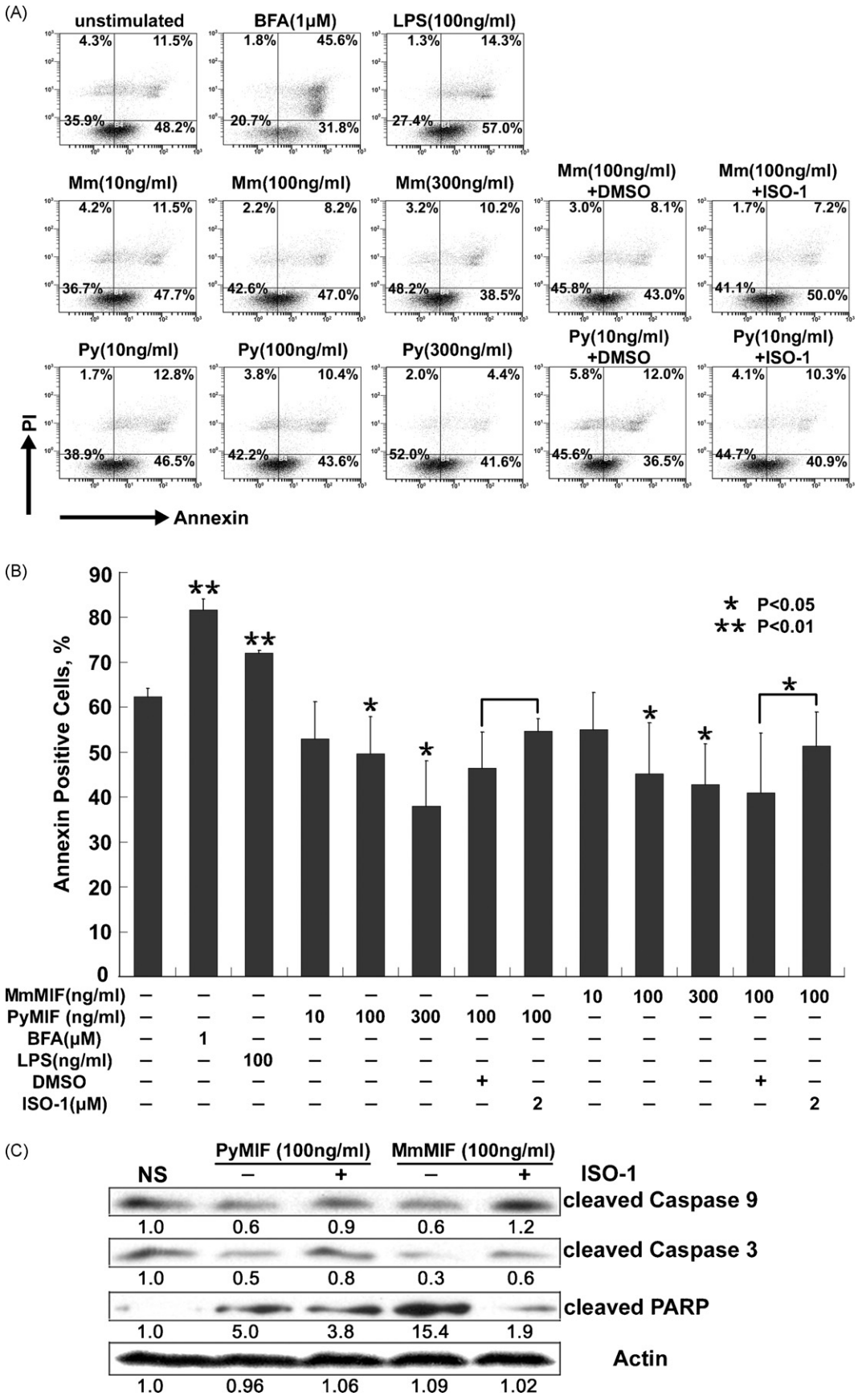

Fig. 5. MIF prolongs or improves RAW264.7 cell survival *in vitro*. (A) RAW264.7 cells were incubated in the presence or absence of PyMIF or MmMIF at various concentrations and in the presence or absence of ISO-1 for 20 h, Brefeldin A (BFA) and lipopolysaccharide (LPS) were used as positive controls. Cell apoptosis was analyzed by propidium iodide and Annexin V staining as described in Section 2. The results presented are representative of three independent experiments. (B) PyMIF and MmMIF have a statistically

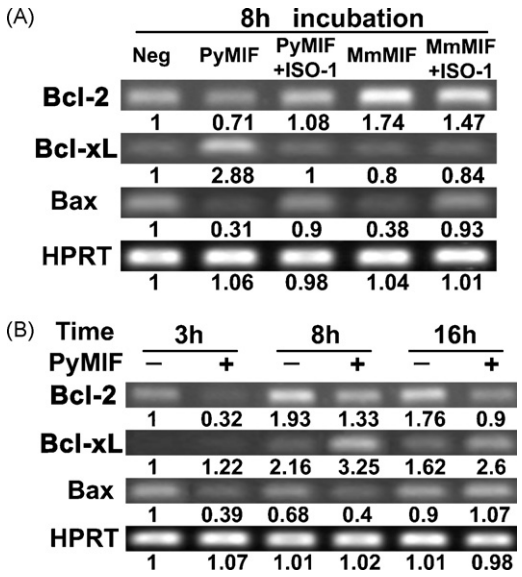

Fig. 6. PyMIF and MmMIF differentially induce Bcl-2 family gene transcription. (A) RAW264.7 cells were incubated in the presence or absence of PyMIF or MmMIF at 100 ng/ml with or without ISO-1 for 8 h. (B) RAW264.7 cells were incubated in the presence or absence of PyMIF at 100 ng/ml for various times. Reverse transcriptase-polymerase chain reaction was performed as described in Section 2. The intensity of the *Bcl-2*, *Bcl-xL*, and *Bax* bands following each treatment were each divided by the intensity of the hypoxanthine phosphoribosyltransferase (*Hprt*) band from the same treatment. The fold activation ratio for each treatment was normalized to the fold activation ratio for the absence of any treatment (set equal to 1).

3.4. PyMIF inhibits mouse macrophage apoptosis in vitro

To investigate the effect of PyMIF on host immune cells, we evaluated its effect on host macrophages. First, we observed that both PyMIF and MmMIF inhibited macrophage apoptosis. At concentrations of 100 and 300 ng/ml, both PyMIF and MmMIF were shown to reduce the number of Annexin V-positive cells and increase the number of live cells, whereas no change was observed when PyMIF and MmMIF were added at lower concentrations (Fig. 5A and B). Moreover, we noticed that the combination of PyMIF and ISO-1 had no statistically significant effect in restoring the Annexin V-positive population, similar to the effect of ISO-1 on the other parasite MIFs (Cho et al., 2007; Kamir et al., 2008). To confirm the apoptosis-inhibiting effect of PyMIF and MmMIF, we evaluated the effects on the levels of three apoptosis associated proteins. Both PyMIF and MmMIF decreased the levels of cleaved caspase 9 and caspase 3 and increased the level of cleaved PARP in macrophages (Fig. 5C). In addition, we found no significant change to the apoptosis effect of PyMIF and MmMIF in a pro-B cell line or in fibroblasts (data not shown).

Although both PyMIF and MmMIF play a role in sustaining macrophage survival, we noticed that PyMIF induced more gene transcription than did MmMIF (Signal Transduction Pathway Finder Array, unpublished observation). According to the microarray and further transcriptional analysis, PyMIF and MmMIF appeared to modulate anti-apoptosis molecules differently such as *Bcl-xL* and *Bcl-2*, however, both of them downregulated *Bax* (Fig. 6A). Moreover, the time-tracing experiments showed that the transcription levels of *Bcl-2*, *Bcl-xL*, and *Bax* modulated by PyMIF were dynamically changed (Fig. 6B).

3.5. PyMIF and MmMIF exhibit a synergistic effect at low concentrations and a suppressive effect at high concentrations on activating the macrophage MAPK pathway

Previous experiments showed that PyMIF could induce ERK1/2-MAPK and PI3K/AKT activation in fibroblasts, and we confirmed that PyMIF could activate the ERK1/2-MAPK pathway in macrophages (Fig. S5). During infection, parasite MIF and host MIF exist together within the host, giving rise to the question of how they might influence the activity of one another. First, we treated NIH/3T3 cells with both PyMIF and MmMIF at various concentrations and evaluated the phosphorylation of Erk1/2 or Akt (Fig. 7A). We found that there was a greater level of Erk1/2 and Akt phosphorylation following treatment with 1 ng/ml PyMIF plus 1 ng/ml MmMIF than when either cytokine was administered alone. Moreover, the level of Erk1/2 phosphorylation following administration of 100 ng/ml PyMIF plus 100 ng/ml MmMIF was lower than that induced by the 1 ng/ml combination, indicating a dynamic and complicated combinatorial effect. We next investigated whether the combinatorial effect existed in macrophages and found a similar modulating effect in RAW264.7 cells (Fig. 7B). These results indicated that the combinatorial effect induced by the two MIFs was not "the more the better" or "the more the worse"; instead, there was a synergistic effect at the lower concentration and a suppressive effect at the higher concentration.

3.6. Injection of recombinant PyMIF in vivo up-regulates several proinflammatory cytokines and delays death

To investigate the role of PyMIF during infection *in vivo*, Balb/c mice were injected intravenously after challenge with 200 ng recombinant PyMIF and 200 ng OVA as control. No change was observed when we injected the mice with rPyMIF at early stage of infection (data not shown). Then we analyzed the effect of injection on middle stage, including once on day 4 or day 5, or once each on days 4 and 5 post-parasite challenge. Relative to the control group, the treated groups showed mildly prolonged survival and parasitemia (Fig. 8A). Furthermore, we detected that the levels of six cytokines were elevated in infected mice. Although the levels of all of these cytokines were shown to be higher in recombinant PyMIF-injected mice than that in the control group, only the elevations of TNFα ($p < 0.05$) and IL-6 ($p < 0.01$) were statistically significant (Fig. 8B).

4. Discussion

Molecular model and catalytic site analyses of several other parasite-derived MIFs have showed a global topology that is similar to the host MIF (Cho et al., 2007; Kamir et al., 2008; Tan et al., 2001; Zang et al., 2002), however, by crystallizing PyMIF in complex with a tautomerase substrate, HPP, here, for the first time, we find that the binding patterns between the parasite-derived and mammalian-derived MIF are completely different. The change in the binding orientation could have led to the lower level of HPP tautomerase activity in PyMIF. Moreover, these altered binding features may account for the decreased effect of the mammalian MIF-specific inhibitor ISO-1 on PyMIF. In our experiments, ISO-1 only partially inhibited PyMIF in the signal transduction and cell fate assays. The binding mechanism of ISO-1 with mammalian MIF was very similar to that of HPP with host MIF (Lubetsky et al., 1999, 2002); there-

significant anti-apoptosis effect on RAW264.7 cells at 100 and 300 ng/ml as compared to negative controls. The effect of MmMIF was restored by ISO-1 treatment while that of PyMIF was not. Asterisks indicate $p < 0.05$ and double asterisks indicate $p < 0.01$ ($n = 4$). (C) RAW264.7 cells were incubated in the presence or absence of PyMIF or MmMIF at 100 ng/ml with or without ISO-1 for 20 h; cleaved caspase 9, cleaved caspase 3, and cleaved PARP were detected by western analysis. Numbers indicate relative density ratios.

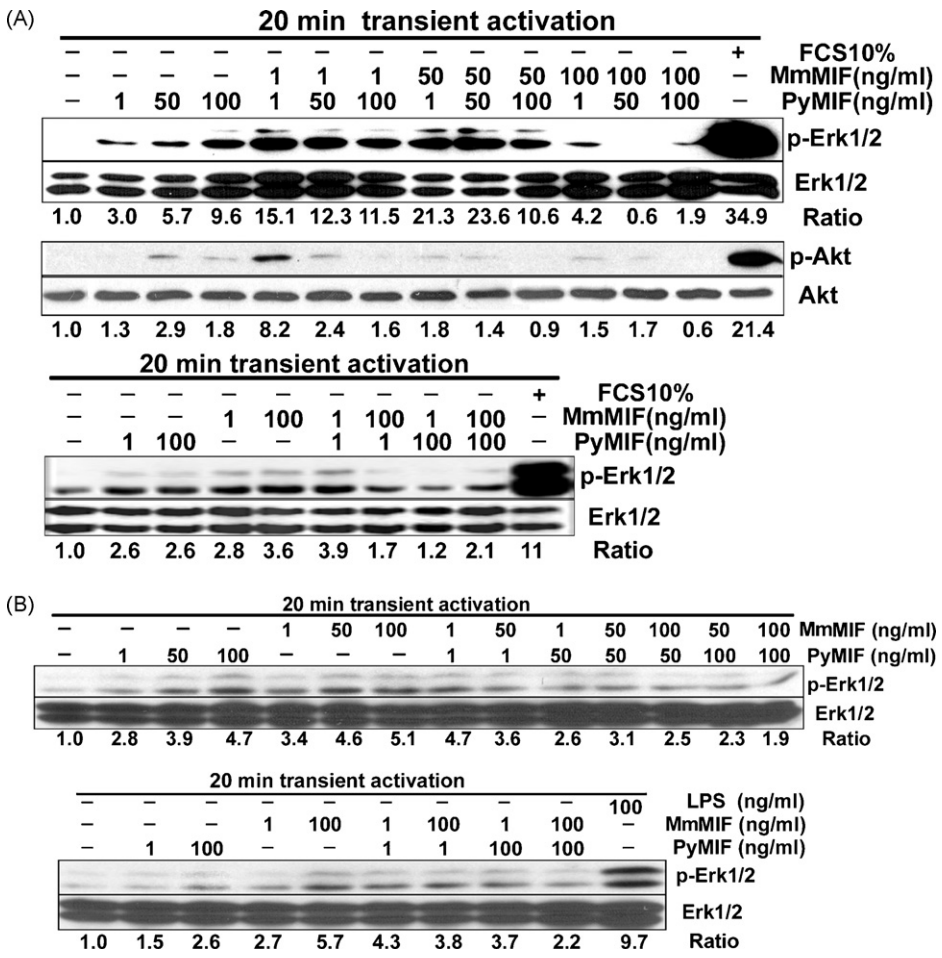

Fig. 7. PyMIF and MmMIF exhibit a synergistic effect at low concentration and an antagonistic effect at high concentration on PI3K/AKT and MAPK pathway activation. (A) NIH/3T3 cells were stimulated with both PyMIF and MmMIF at various concentrations, and Erk1/2 and Akt phosphorylation were analyzed by western analysis. Total Erk1/2 or Akt protein was used for standardization, respectively. (B) RAW264.7 cells were stimulated with both PyMIF and MmMIF at various concentrations, and Erk1/2 phosphorylation was analyzed by western analysis. Total Erk1/2 protein was used for standardization.

fore, our structural analysis could explain the decreased inhibitory effect of ISO-1 on PyMIF activity.

In this study, by detecting PyMIF in all inbred and outbred mice infected by *P. yoelii* for several times, we confirmed that this molecule was released into circulation of host by the parasite after invading the erythrocytes; and its elevated serum level paralleled with the parasitemia till one day before the death of the host. Our data indicate that the parasite-derived MIF must be exist together with its host's MIF, MmMIF, during the infection, though the reason for the "last day decline" of PyMIF still needs further explorations. The variation of host MIF in malaria infection has been reported by others in either human or in animal models. Martiney et al. have showed that the highest serum level of MmMIF in a *P. chabaudi* infected rodent model was lower than 18 ng/ml (Martiney et al., 2000). Later, McDevitt et al. reported that in wild-type mice, plasma MIF concentration was 40 ± 20 ng/ml at day 8 post-*P.chabaudi* infection (McDevitt et al., 2006). Since both of these MmMIF concentrations were associated with infection by a non-lethal strain and the parasite species used were differed from that used in the present study, the concentration and kinetic regulation of MmMIF in our model remains to be addressed once a monoclonal MmMIF antibody is available. Moreover, we noticed that Meyer-Siegler et al. (2005) reported that a significant amount of MIF complexes existing in human serum did not bind to the MIF capture antibody in ELISA experiments, suggesting that the epitope on the surface of the MIF complex might not be accessible to the capture antibody used in routine experiments. If this is also the case in our experiments, the actual serum concentrations of both PyMIF and MmMIF could be greater than what having been detected, which will explain the much higher concentration having to be used to activate cell signal transduction *in vitro*.

Mammalian MIF can regulate many types of immune cells, including macrophages, T lymphocytes, and NK cells. Studies on the target cells of parasite-derived MIFs have focused predominately on the modulation of host macrophages and the role of BmMIF-1 in eosinophil recruitment. Macrophages are the specific cells infected by some parasites, such as *Leishmania* and *Toxoplasma*. More importantly, as major participants in the innate immune response, macrophages play a pivotal role in mediating protection against parasite infection. In this study, we are the first to analyze the whole picture of malaria parasite-derived MIF on almost all important signaling pathways of host cells, and we found that the activities of PyMIF on these pathways were all similar with that of MmMIF. Our result on AP-1 associated signal transduction pathway was similar with the work on PfMIF and PbMIF (Augustijn et al., 2007), and we further confirmed that the effective concentration of PyMIF (between 100 pM and 10 nM) is within the region of the PyMIF serum level that we have detected *in vivo* during malaria infection. Meanwhile, the effects of PyMIF on the signaling pathways, such as MAPK/ERK and PI3K/AKT, were found to be weaker and more transient than that of the MmMIF, looking like it can be "sheltered" by the activity of the latter and therefore, questioning the necessity of this non-significant molecule to be persistently released during malaria infection. Nevertheless, considering the

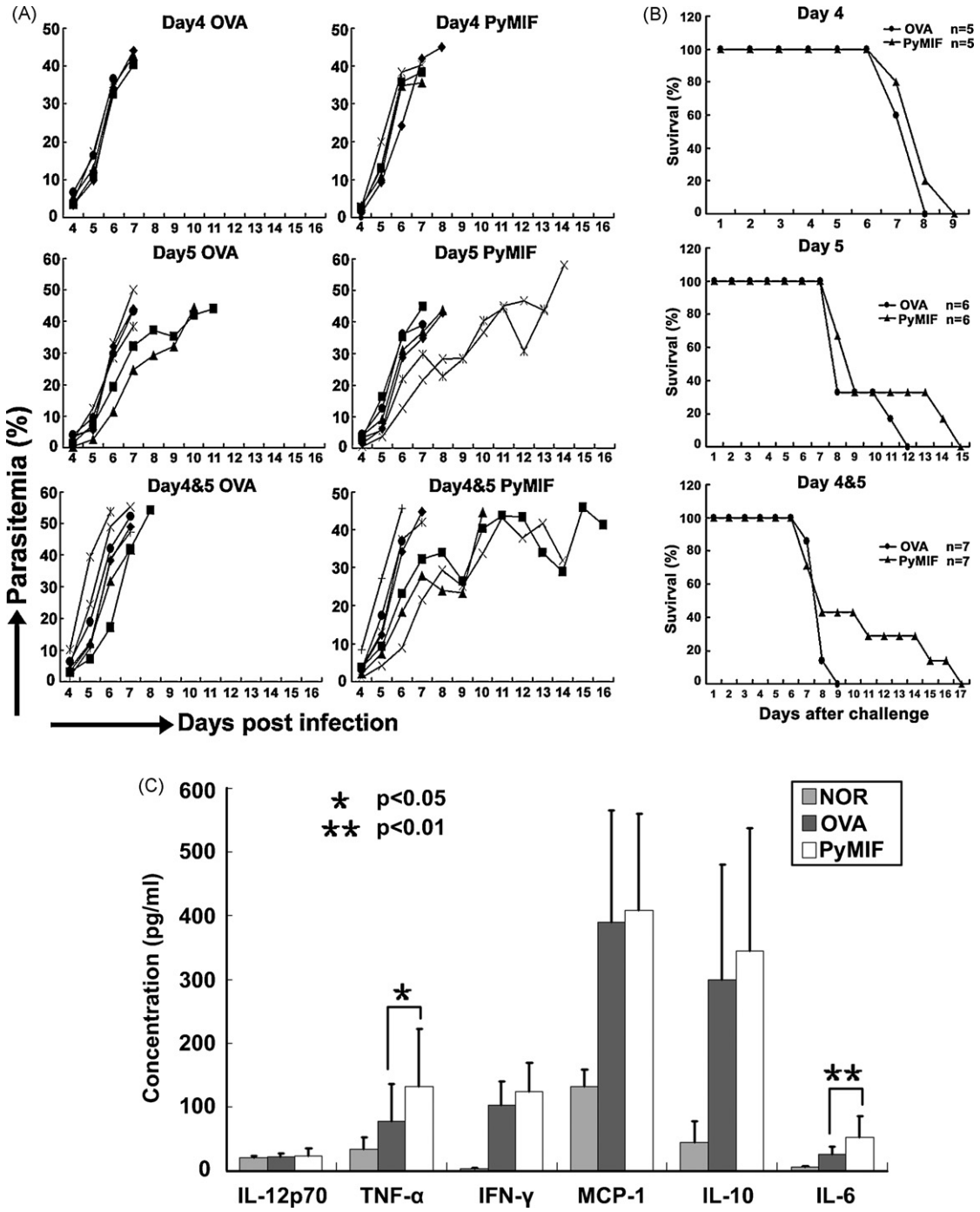

Fig. 8. PyMIF prolongs the survival of Balb/c mice infected with a lethal *P. yoelii* strain and up-regulates the levels of TNF-α and IL-6 *in vivo*. (A) Balb/c mice ($n \geq 5$) were challenged with 2×10^5 *P. yoelii 17XL*, then intravenously injected with 200 ng of recombinant PyMIF once on day 4 or 5 or once each on days 4 and 5, parasitemia was determined in blood smears, negative controls were treated with ovalbumin (OVA). Each curve presents one mouse. (B) The survival curves of mice, corresponding to the results on (A). (C) Balb/c mice ($n \geq 15$) were performed as described above, and the serum levels of six cytokines were detected 36 h after the last injection. Asterisks indicate $p < 0.05$ and double asterisks indicate $p < 0.01$.

two cytokines existing at the same time during malaria infection, to investigate the combination effect of them becomes a crucial step. The synergistic effect of PyMIF plus MmMIF on host signal transduction at such a low concentrations (1 ng/ml of each) indicated that the parasite-derived MIF can 'boost' the effect of the host MIF and activate macrophages in the early stage of malaria infection. More interestingly, when the concentrations of the two MIFs increase in parallel, the effect became the opposite, suggesting that an antagonistic effect might exist later during blood-stage infection. The mechanism for these effects requires further evaluation.

In our previous microarray studies, we found that in macrophages, the parasite- and host-derived MIFs did not modulate the same downstream effectors in multiple signaling pathways; more gene transcription changes were observed in the cells treated with PyMIF than in cells treated with the host homologue (X. Zhong, unpublished). This observation, together with the complex effect induced by the combination of PyMIF and MmMIF, suggests that the parasite and host MIFs might use distinct modes for binding to the receptor. In addition, the distinctive differences in surface electrostatic potential between PyMIF and MmMIF (Fig. S6)

might be associated with difference in receptor binding activity. Therefore, it is important to explore the difference of the molecular mechanism between PyMIF and MmMIF on interacting with receptors in the future.

Host MIF plays an essential role in innate immunity by stimulating the production of multiple inflammatory molecules and cytokines, thereby either enhancing the immune response to eliminate the parasite or, in some cases, eliciting a pathogenic immune response that results in the death of the host. Our results showed that PyMIF activated macrophages *in vitro*, elevated TNF-α and IL-6 *in vivo,* and slightly prolonged the survival of infected mice. These data suggest that PyMIF could act as a pro-inflammatory player, help for the persistence of parasitemia and moderate the anti-parasite immune attacks. However, because *Plasmodium* MIF has been found to be expressed throughout the parasite's life cycle (Augustijn et al., 2007), its behavior during the blood-stage might not represent its overall profile. Furthermore, the roles of MIF from diverse parasite strains, such as lethal versus non-lethal, might not be identical and need future studies.

In conclusion, we have revealed distinctive features of the molecule structure of the *Plasmodium*-derived MIF that could explain the differences in enzyme activity and effects on signal transduction between parasite-derived and host-derived MIFs. In addition, data from both *in vitro* and *in vivo* experiments indicate a role for PyMIF in modulating the host immune response during malaria infection, ultimately increasing the opportunity of the parasite to complete its life cycle. The data presented here will help our understanding of host-parasite interactions and shed new light on the mechanisms of host protection and parasite evasion.

Acknowledgements

We would like to thank Professor Wenhui Li, Xiaozhong Peng, and Hongbing Zhang for training and assistance in conducting the experiments, helpful advice and discussion, and critical reading and comments on the manuscript, Dr. Tom Lee for his helpful advice in revising the manuscript, Professor Qijun Chen and Xin-zhuan Su for helpful advice and discussion, and Lanlan Gu for her help in cytokine detection in mice sera. The authors have no conflicting financial interests with regard to any topic or product included in this manuscript.

This work was supported by research grants from the National Basic Research Program of China (973 Program) #2007CB513100, the Natural Science Foundation of China #30700761.

Appendix A. Supplementary data

Supplementary data associated with this article can be found, in the online version, at doi:10.1016/j.molimm.2009.10.037.

References

Amin, M.A., Haas, C.S., Zhu, K., Mansfield, P.J., Kim, M.J., Lackowski, N.P., Koch, A.E., 2006. Migration inhibitory factor up-regulates vascular cell adhesion molecule-1 and intercellular adhesion molecule-1 via Src, PI3 kinase, and NFkappaB. Blood 107, 2252–2261.

Augustijn, K.D., Kleemann, R., Thompson, J., Kooistra, T., Crawford, C.E., Reece, S.E., Pain, A., Siebum, A.H., Janse, C.J., Waters, A.P., 2007. Functional characterization of the Plasmodium falciparum and P. berghei homologues of macrophage migration inhibitory factor. Infect. Immun. 75, 1116–1128.

Awandare, G.A., Ouma, Y., Ouma, C., Were, T., Otieno, R., Keller, C.C., Davenport, G.C., Hittner, J.B., Vulule, J., Ferrell, R., Ong'echa, J.M., Perkins, D.J., 2007. Role of monocyte-acquired hemozoin in suppression of macrophage migration inhibitory factor in children with severe malarial anemia. Infect. Immun. 75, 201–210.

Bernhagen, J., Mitchell, R.A., Calandra, T., Voelter, W., Cerami, A., Bucala, R., 1994. Purification, bioactivity, and secondary structure analysis of mouse and human macrophage migration inhibitory factor (MIF). Biochemistry 33, 14144–14155.

Cho, Y., Jones, B.F., Vermeire, J.J., Leng, L., DiFedele, L., Harrison, L.M., Xiong, H., Kwong, Y.K., Chen, Y., Bucala, R., Lolis, E., Cappello, M., 2007. Structural and functional characterization of a secreted hookworm macrophage migration inhibitory factor (MIF) that interacts with the human MIF receptor CD74. J. Biol. Chem. 282, 23447–23456.

Cordery, D.V., Kishore, U., Kyes, S., Shafi, M.J., Watkins, K.R., Williams, T.N., Marsh, K., Urban, B.C., 2007. Characterization of a Plasmodium falciparum macrophage-migration inhibitory factor homologue. J. Infect. Dis. 195, 905–912.

Emsley, P., Cowtan, K., 2004. Coot: model-building tools for molecular graphics. Acta Crystallogr. D: Biol. Crystallogr. 60, 2126–2132.

Fernandes, A.A., Carvalho, L.J., Zanini, G.M., Ventura, A.M., Souza, J.M., Cotias, P.M., Silva-Filho, I.L., Daniel-Ribeiro, C.T., 2008. Similar cytokine responses and degrees of anemia in patients with Plasmodium falciparum and Plasmodium vivax infections in the Brazilian Amazon region. Clin. Vac. Immunol. 15, 650–658.

Flores, M., Saavedra, R., Bautista, R., Viedma, R., Tenorio, E.P., Leng, L., Sanchez, Y., Juarez, I., Satoskar, A.A., Shenoy, A.S., Terrazas, L.I., Bucala, R., Barbi, J., Satoskar, A.R., Rodriguez-Sosa, M., 2008. Macrophage migration inhibitory factor (MIF) is critical for the host resistance against Toxoplasma gondii. FASEB J. 22, 3661–3671.

Gore, Y., Starlets, D., Maharshak, N., Becker-Herman, S., Kaneyuki, U., Leng, L., Bucala, R., Shachar, I., 2008. Macrophage migration inhibitory factor induces B cell survival by activation of a CD74–CD44 receptor complex. J. Biol. Chem. 283, 2784–2792.

Juttner, S., Bernhagen, J., Metz, C.N., Rollinghoff, M., Bucala, R., Gessner, A., 1998. Migration inhibitory factor induces killing of Leishmania major by macrophages: dependence on reactive nitrogen intermediates and endogenous TNF-alpha. J. Immunol. 161, 2383–2390.

Kabsch, W., 1993. Automatic processing of rotation diffraction data from crystals of internally unknown symmetry and cell constants. J. Appl. Cryst. 26, 795–800.

Kamir, D., Zierow, S., Leng, L., Cho, Y., Diaz, Y., Griffith, J., McDonald, C., Merk, M., Mitchell, R.A., Trent, J., Chen, Y., Kwong, Y.K., Xiong, H., Vermeire, J., Cappello, M., McMahon-Pratt, D., Walker, J., Bernhagen, J., Lolis, E., Bucala, R., 2008. A Leishmania ortholog of macrophage migration inhibitory factor modulates host macrophage responses. J. Immunol. 180, 8250–8261.

Kleemann, R., Hausser, A., Geiger, G., Mischke, R., Burger-Kentischer, A., Flieger, O., Johannes, F.J., Roger, T., Calandra, T., Kapurniotu, A., Grell, M., Finkelmeier, D., Brunner, H., Bernhagen, J., 2000. Intracellular action of the cytokine MIF to modulate AP-1 activity and the cell cycle through Jab1. Nature 408, 211–216.

Koebernick, H., Grode, L., David, J.R., Rohde, W., Rolph, M.S., Mittrucker, H.W., Kaufmann, S.H., 2002. Macrophage migration inhibitory factor (MIF) plays a pivotal role in immunity against Salmonella typhimurium. Proc. Natl. Acad. Sci. U.S.A. 99, 13681–13686.

Lubetsky, J.B., Dios, A., Han, J., Aljabari, B., Ruzsicska, B., Mitchell, R., Lolis, E., Al-Abed, Y., 2002. The tautomerase active site of macrophage migration inhibitory factor is a potential target for discovery of novel anti-inflammatory agents. J. Biol. Chem. 277, 24976–24982.

Lubetsky, J.B., Swope, M., Dealwis, C., Blake, P., Lolis, E., 1999. Pro-1 of macrophage migration inhibitory factor functions as a catalytic base in the phenylpyruvate tautomerase activity. Biochemistry 38, 7346–7354.

Lue, H., Thiele, M., Franz, J., Dahl, E., Speckgens, S., Leng, L., Fingerle-Rowson, G., Bucala, R., Luscher, B., Bernhagen, J., 2007. Macrophage migration inhibitory factor (MIF) promotes cell survival by activation of the Akt pathway and role for CSN5/JAB1 in the control of autocrine MIF activity. Oncogene 26, 5046–5059.

Martiney, J.A., Sherry, B., Metz, C.N., Espinoza, M., Ferrer, A.S., Calandra, T., Broxmeyer, H.E., Bucala, R., 2000. Macrophage migration inhibitory factor release by macrophages after ingestion of Plasmodium chabaudi-infected erythrocytes: possible role in the pathogenesis of malarial anemia. Infect. Immun. 68, 2259–2267.

McDevitt, M.A., Xie, J., Shanmugasundaram, G., Griffith, J., Liu, A., McDonald, C., Thuma, P., Gordeuk, V.R., Metz, C.N., Mitchell, R., Keefer, J., David, J., Leng, L., Bucala, R., 2006. A critical role for the host mediator macrophage migration inhibitory factor in the pathogenesis of malarial anemia. J. Exp. Med. 203, 1185–1196.

Meyer-Siegler, K.L., Iczkowski, K.A., Vera, P.L., 2005. Further evidence for increased macrophage migration inhibitory factor expression in prostate cancer. BMC Cancer 5, 73.

Painter, J., Merritt, E.A., 2006. Optimal description of a protein structure in terms of multiple groups undergoing TLS motion. Acta Crystallogr. D: Biol. Crystallogr. 62, 439–450.

Pastrana, D.V., Raghavan, N., FitzGerald, P., Eisinger, S.W., Metz, C., Bucala, R., Schleimer, R.P., Bickel, C., Scott, A.L., 1998. Filarial nematode parasites secrete a homologue of the human cytokine macrophage migration inhibitory factor. Infect. Immun. 66, 5955–5963.

Rodriguez-Sosa, M., Rosas, L.E., David, J.R., Bojalil, R., Satoskar, A.R., Terrazas, L.I., 2003. Macrophage migration inhibitory factor plays a critical role in mediating protection against the helminth parasite Taenia crassiceps. Infect. Immun. 71, 1247–1254.

Sashinami, H., Sakuraba, H., Ishiguro, Y., Munakata, A., Nishihira, J., Nakane, A., 2006. The role of macrophage migration inhibitory factor in lethal Listeria monocytogenes infection in mice. Microb. Pathog. 41, 111–118.

Satoskar, A.R., Bozza, M., Rodriguez Sosa, M., Lin, G., David, J.R., 2001. Migration-inhibitory factor gene-deficient mice are susceptible to cutaneous Leishmania major infection. Infect. Immun. 69, 906–911.

Shao, D., Han, Z., Lin, Y., Zhang, L., Zhong, X., Feng, M., Guo, Y., Wang, H., 2008. Detection of Plasmodium falciparum derived macrophage migration inhibitory factor homologue in the sera of malaria patients. Acta Trop. 106, 9–15.

Swope, M., Sun, H.W., Blake, P.R., Lolis, E., 1998. Direct link between cytokine activity and a catalytic site for macrophage migration inhibitory factor. EMBO J. 17, 3534–3541.

Tan, T.H., Edgerton, S.A., Kumari, R., McAlister, M.S., Roe, S.M., Nagl, S., Pearl, L.H., Selkirk, M.E., Bianco, A.E., Totty, N.F., Engwerda, C., Gray, C.A., Meyer, D.J., 2001. Macrophage migration inhibitory factor of the parasitic nematode Trichinella spiralis. Biochem. J. 357, 373–383.

Vagin, A., Teplyakov, A., 1997. MOLREP: an automated program for molecular replacement. J. Appl. Crystallogr. 30, 1022–1025.

Winn, M.D., Isupov, M.N., Murshudov, G.N., 2001. Use of TLS parameters to model anisotropic displacements in macromolecular refinement. Acta Crystallogr. D: Biol. Crystallogr. 57, 122–133.

Zang, X., Taylor, P., Wang, J.M., Meyer, D.J., Scott, A.L., Walkinshaw, M.D., Maizels, R.M., 2002. Homologues of human macrophage migration inhibitory factor from a parasitic nematode. Gene cloning, protein activity, and crystal structure. J. Biol. Chem. 277, 44261–44267.